International Journal of Solids and Structures 56–57 (2015) 53–61

Contents lists available at ScienceDirect

International Journal of Solids and Structures

journal homepage: www.elsevier.com/locate/ijsolstr

The role of the sliding direction against a grooved channel texture on tool steel: An experimental study on tactile friction

Sheng Zhang [a,1,*], Adriana Rodriguez Urribarri [a,1], Marina Morales Hurtado [a], Xiangqiong Zeng [a], Emile van der Heide [a,b]

[a] Laboratory for Surface Technology and Tribology, Faculty of Engineering Technology, University of Twente, Drienerlolaan 5, 7522 NB Enschede, The Netherlands
[b] TNO, P.O. Box 6235, 5600 HE Eindhoven, The Netherlands

ARTICLE INFO

Article history:
Received 30 July 2014
Received in revised form 27 November 2014
Available online 10 December 2014

Keywords:
Skin tribology
Tactile friction
Surface texture
Sliding direction

ABSTRACT

To control tactile friction, that is the friction between fingertip and counter-body, the role of surface texture is required to be unveiled and defined. In this research, an experimental approach is used based on measuring tactile friction for directional texture (grooved channel) with varying depths. For a reference surface, in this current case a polished surface from the same tool steel is compared. The experimental results are analyzed to explain the observed skin friction behavior as a function of surface texture parameters, sliding direction and applied normal load. Sliding parallel to the groove length shows greater values in COF than sliding perpendicular to the groove direction. Furthermore, parallel sliding reveals a higher dependency of COF on the depth of the grooved channel texture than perpendicular sliding. Application of the two term friction model suggests that the adhesion component of friction has greater impact on parallel than perpendicular sliding direction. According to the observations, grooved channels are well suited to control skin friction in direction dependent sliding, for moderately loaded contact situations. This experimental research contributes to the haptic perception related research, and to the development of other direction-dependent surface structures for touch.

1. Introduction

The study of friction and the role of surface textures in relation to touch perception is the subject of researches in both science and industry for a wide variety of applications (van Kuilenburg et al., 2013; Derler et al., 2009; van der Heide et al., 2013). Tactility is directly related to the functional behavior and perception of products like haptic devices, smartphone cases, tool handles, personal care products and for example kitchenware. In most cases, the exploratory procedure to detect the surface features of various objects consists of a sliding movement of our finger(s) at a moderate load and relatively low sliding velocity (Klatzky and Pawluk, 2013; Barnes et al., 2004). Surface recognition is deciphered by the cutaneous sensory neurons from the specific movement made by our finger during active touch (Fagiani et al., 2012). The touch perception is greatly influenced by the friction generated between the fingertip and counter-surfaces (Darden and Schwartz, 2013; Klatzky and Pawluk, 2013; Liu et al., 2008; Skedung et al., 2011).

Perception can be linked to psychophysical factors such as smooth-rough, slippery-grippy, warm-cold and soft-hard (Liu et al., 2008). The frictional behavior of skin-surface sliding is important in all of these factors (Kuramitsu et al., 2013). Tactile friction requires an in-depth understanding of the contact mechanics and the behavior of human skin. Surface textures can be categorized as deterministic nature or as stochastic nature (Steinhoff et al., 1996). Deterministic textures have a repetition of fixed geometric structure, and stochastic textures are non-deterministic with random surface pattern. Stochastic surfaces typically use roughness parameters based on distribution characteristics and could result in surfaces that are distinctively different in pattern, yet which have the same distribution parameters. In the work of Skedung (Skedung et al., 2011), finger friction measurements are evaluated to determine the relationship between the coefficient of friction (COF) and surface roughness of a series of printing papers. The research found that both roughness and finger friction can be related to perceived coarseness. The topography of paper samples is stochastic and directional-independent. As the relation between distribution related parameters and touch functionality is not known, it seems likely that progress can only be made in this field by using surfaces with pre-defined features. These

* Corresponding author. Tel.: +31 (0) 6 33976966; fax: +31 (0)53 489 4784.
E-mail address: s.zhang@utwente.nl (S. Zhang).
[1] Contributed equally to this work.

http://dx.doi.org/10.1016/j.ijsolstr.2014.12.005
0020-7683/

pre-defined features with deterministic nature are better controlled for touch functionality related experiments.

In this research, the directional texture like grooved channel is designed as deterministic surface structures for the purpose of studying the role of sliding direction for tactile friction. The finger friction tests are performed on the steel samples with directional textures. The structures are fabricated as grooved channels by using laser surface texturing technology. The objective is to find the relation between surface topography parameters and COF with the influence of sliding directions (perpendicular and parallel) on directional textures.

2. Skin tribology

Human skin has a layered and complex structure. Each skin layer has a different composition, thickness and hydration degree which results in different mechanical properties (Morales Hurtado et al., 2014). Consequently, the full skin structure shows a viscoelastic, non-homogeneous, nonlinear, anisotropic behavior when skin is under load.

Basically, skin is composed of 3 layers: epidermis, dermis and hypodermis. The stratum corneum is the outermost layer of epidermis which is directly in contact with the surrounding environment. It has an important role in hydration control and tactile friction (Tagami and Yoshikuni, 1985). The next layer in the skin structure is dermis. Sensory receptors have their origin in this layer which have a role in the tribological response (Silver et al., 1992; Edwards and Marks, 1995). Hypodermis is the deepest layer of the human skin. Its role in skin mechanical properties could be neglected for tactile application (Ramsay, 1996). Skin's response to stress depends on the combined behavior of these layers. In addition, the state and properties are a function of the body site, age, degree of hydration or nutritional conditions (Lapière, 1990; Hendriks and Franklin, 2010; Derler et al., 2009; Diridollou et al., 2001; Cua et al., 1990; Veijgen et al., 2013). As a result, a specific value for tribo mechanical properties of skin, cannot be given.

The relationship between skin structure, hydration and skin friction response is the subject of several experimental studies, see e.g. the work of Derler (Derler and Gerhardt, 2012). From the review, it is concluded that for both dry and humid conditions, the adhesion component is dominant in sliding contacts between skin and other surfaces. In this research, the experiments are conducted based on the skin in dry conditions, because most sliding touches for consumers' products occur in dry conditions.

The friction force (F_f) between human skin and a counter-surface can be composed of an adhesive term ($F_{f,adh}$) and a term resulting from deformation ($F_{f,def}$) as in Eq. (1) (Greenwood and Tabor, 1958).

$$F_{f,tot} = F_{f,adh} + F_{f,def} \tag{1}$$

The adhesion force from Eq. (1) can be predicted by the following equations (Greenwood and Tabor, 1958; Johnson et al., 1993; Adams et al., 2007).

$$F_{f,adh} = \tau \cdot A_{real} \tag{2}$$

Where A_{real} is the real contact area; τ is the shear strength of the interface.

The deformation term depends on the actual contact situation. The real contact area is more important compared to apparent contact area in order to predict the friction due to adhesion component of friction and it is difficult to be measured experimentally (Derler et al., 2014). The apparent contact area is defined as the area of the fingertip in contact with the counter-surface (Bowden and Tabor, 1950; van Kuilenburg et al., 2012). The real contact area is constituted by the sum of all contacted spots between two surfaces and it is a function of surface texture, material properties and interfacial loading conditions (Bowden and Tabor, 1950; Zahouani et al., 2011).

3. Experimental method

3.1. Materials

The experimental work was conducted by using samples from tool steel WN 1.2510. The grooved channels with varying depths D (see Fig. 1) were produced as the deterministic pattern by using laser surface texturing technology. The surface topography of each sample was examined by using a confocal laser scanning microscope (VK 9700 KEYENCE, Japan) (refer to Table 1). For the sample with stochastic surface roughness, arithmetic mean (Ra), the root-mean-square roughness (Rq) and maximum peak to valley height (Rz) were obtained from the surface area. Deterministic surface patterns were described by the top to valley distance (D), spacing (λ) and width (w), and the surface roughness and horizontal distance for the high portions on the top of the grooves are shown as well.

3.2. Experimental set-up and preparation

Friction measurements on skin in vivo were carried out by using a load cell (ATI Gamma three-axis force/torque transducer, ATI Industrial Automation, Apex, NC, USA). The ATI force transducer uses six degrees of freedom to measure the forces (normal force in z-direction, tangential forces in xy-plane and torques around x, y and z axes). The force measurements have a resolution of 25 mN in normal direction and 12.5 mN in tangential direction, with a sampling rate of 100 Hz. The sliding velocity was calculated from the displacement of initial contact position and final position over time.

Each sample was fixed to the top of the friction transducer using double sided tape. For the group of samples with deterministic surfaces, each counter-body was aligned with a parallel or perpendicular orientation to that of the moving axis of the finger. The middle finger of the non-dominant (left) hand of a healthy female adult (25 years old) was used for all the experiments reported here. One experiment consisted of three repetitive single strokes of the finger, sliding towards the body. The stroke length on each sample depended on the size of the surface and shape. For the samples with deterministic surface pattern, the stroke length was 25 mm. For the samples with stochastic surface pattern, the stroke length was 45 mm.

The normal load was controlled by placing a mass on the top of the sliding finger as shown in Fig. 2(a). Once the normal load was

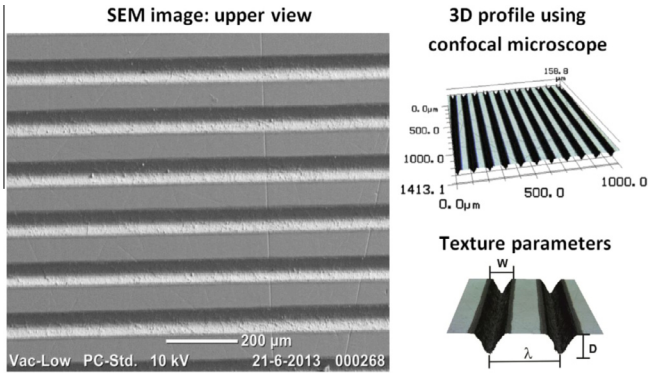

Fig. 1. Grooved channel texture on tool steel samples (a) SEM image: upper view; (b) 3D profile using confocal microscope; (c) texture parameters.

Table 1
The surface parameters of the samples. For the group of samples with stochastic surface roughness, arithmetic mean (Ra), the root-mean-square roughness (Rq) and maximum peak to valley height (Rz) were obtained from the surface area. Deterministic surface patterns were described by the top to valley distance (D), spacing (λ), width (w) and for the high portions on the top of the grooves the Ra, Rq, Rz and horizontal distances, were obtained from the surface area.

Deterministic structures							
Sample No.	Depth D [μm]	Spacing λ [μm]	Width w [μm]	Ra [μm]	Rq [μm]	Rz [μm]	Horz. Dist. [μm]
S001	30	100	45	0.06	0.07	0.90	48.4
S002	15	100	45	0.09	0.10	2.00	46.7
S003	5	100	45	0.04	0.05	1.03	46.4

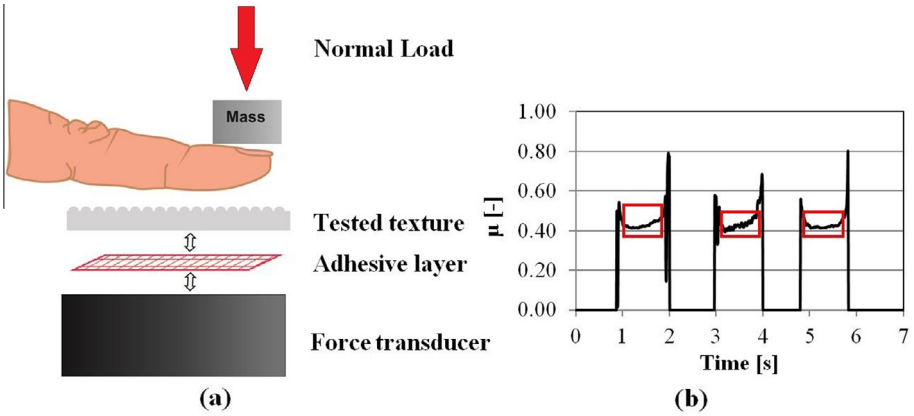

Fig. 2. Description of the experimental procedure:(a) test set-up; (b) measurements of friction.

comfortably placed over the skin area tested, each stroke started with imminent movement of the fingertip against the surface tested. During each stroke, the sliding velocity was kept as constant as possible. The end of each stroke was determined when there was no contact anymore, or when the normal load was equal to zero. Coefficients of friction (COF) were calculated within a selected range with respect to the targeted normal load (0.5 N, 1 N and 2 N). In this way, the data at the beginning and the end of each stroke was excluded as shown in Fig 2 (b) below. An average velocity of 37 ± 8 mm/s was employed in all the experiments reported in this work. This window of operational conditions was taken as representative of those used when exploring a surface with a finger (Liu et al., 2008). All measurements were carried out in an environmentally controlled laboratory at 20 ± 1 °C and 40 ± 5% relative humidity. Before each experiment, the subject cleaned her finger with a tissue in combination with an amount of isopropanol to remove any sweat from most of the upper surfaces of the ridges of the skin. The hydration level of the skin surface was monitored before the measurements using a Corneometer CM 825 (Courage + Khazaka GmbH, Germany). The average hydration level of the skin was 40 ± 3 AU. This level is typical for 'dry' conditions (Heinrich et al., 2003) (See Table 2).

Table 2
Experimental data for deterministic and stochastic surfaces in both perpendicular and parallel sliding direction.

Sliding motion	Sample	Normal load [N] Mean ± STD	COF Mean ± STD	Depth D [μm]
Perpendicular motion (⊥)	S000	0.38 ± 0.10	0.68 ± 0.05	–
	S001	0.44 ± 0.05	0.56 ± 0.04	30
	S002	0.50 ± 0.12	0.54 ± 0.07	15
	S003	0.57 ± 0.10	0.52 ± 0.06	5
	S000	0.97 ± 0.23	0.66 ± 0.03	–
	S001	0.89 ± 0.56	0.62 ± 0.06	30
	S002	0.93 ± 0.08	0.62 ± 0.07	15
	S003	0.83 ± 0.05	0.59 ± 0.04	5
	S000	2.23 ± 0.43	0.75 ± 0.05	–
	S001	2.42 ± 0.22	0.37 ± 0.02	30
	S002	2.39 ± 0.26	0.36 ± 0.02	15
	S003	2.31 ± 0.23	0.41 ± 0.03	5
Parallel motion (//)	S000	0.38 ± 0.04	0.65 ± 0.03	–
	S001	0.34 ± 0.06	1.03 ± 0.12	30
	S002	0.48 ± 0.05	1.33 ± 0.08	15
	S003	0.62 ± 0.11	1.34 ± 0.23	5
	S000	0.97 ± 0.08	0.56 ± 0.05	–
	S001	0.93 ± 0.08	0.93 ± 0.10	30
	S002	0.93 ± 0.05	1.10 ± 0.10	15
	S003	0.81 ± 0.05	1.23 ± 0.11	5
	S000	2.23 ± 0.15	0.85 ± 0.06	–
	S001	2.19 ± 0.14	0.93 ± 0.08	30
	S002	2.07 ± 0.15	1.04 ± 0.15	15
	S003	2.00 ± 0.08	1.17 ± 0.16	5

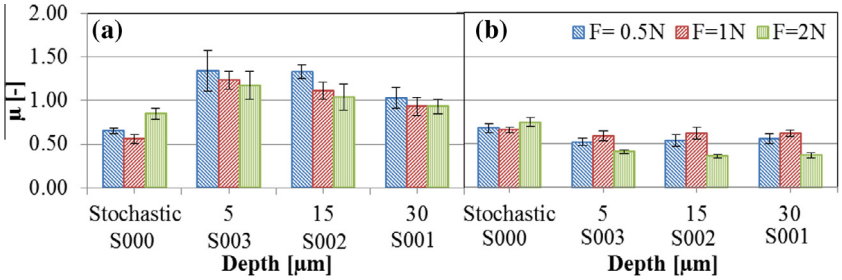

Fig. 3. Overview of COF: (a) motion parallel to groove length and (b) motion perpendicular to groove length, compared to stochastic surface.

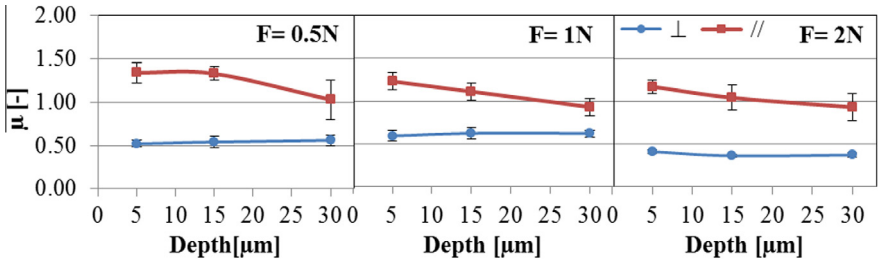

Fig. 4. COF vs. depth for steel samples at different normal loads.

4. Results

For each sample, three friction cycles with one sliding movement in direction 'towards the human body' were analyzed to calculate each COF. The average of COF and its corresponding standard deviation (STD) were calculated from the data obtained from three strokes (Fig. 2 b). Fig. 3 shows an overview of COF measured against dry skin with deterministic and stochastic surfaces in both perpendicular and parallel sliding direction with respect to the groove length. The mean value of dynamic COF is calculated under different normal loads. The standard deviations ranged from 0.01 to 0.2, indicating variations between sliding cycles. COF ranged from 0.9 to 1.3 in the sliding direction parallel to the groove length. Meanwhile COF ranged from 0.3 to 0.7 in the perpendicular sliding direction. The stochastic surface is relatively smooth, and was measured for the purpose of comparison (S000). COF ranged from 0.56 to 0.85 for the stochastic surface in the parallel sliding direction and from 0.62 to 0.75 in the perpendicular sliding direction. The sliding direction used with respect to the surface pattern is defined as "⊥" in perpendicular and "//" in parallel.

5. Discussion

For fingertip sliding on counter-body, Tomlinson (Tomlinson et al., 2009) reported COF of 0.23 for stainless steel. Gee (Gee et al., 2005) investigated the friction of the finger in the left to right direction on different materials, and found COF of 1.75 for steel. COF within this range were also found in the touch experiments presented here: i.e. 0.3–1.3 for steel including both parallel and perpendicular sliding direction.

5.1. The effect of the grooved surface texture

It is expected that COF can vary at the higher normal load level by changing lambda spacing (λ) or the width of grooves, because the contact area of skin varies accordingly (Smith et al., 2002; Taylor and Lederman, 1975; Wang et al., 2008).

Based on the experimental results of this paper, as the depth of grooves increased, the COF for the parallel sliding decreased (refer to Fig. 4). According to the experiments of Skedung et al. (Skedung et al., 2011), a similar phenomenon is observed with various paper samples, as there is an inverse relation found between skin friction and surface roughness. A possible explanation for this phenomenon is that due to the reduced contact area between skin and the counter-surface, the adhesion component of the friction force decreases (refer to Eq. (2)).

A contact model is able to estimate the contact ratio between an elastic half-space and rigid wavy surface with wavelength (λ) and amplitude (the depth of groove, D) (Westergaard 1939; Johnson et al., 1985).

$$\frac{(\lambda - w)}{\lambda} = \frac{2}{\pi}\sin^{-1}\left(\frac{\bar{p}}{p^*}\right)^{1/2} \tag{3}$$

Where λ is the lambda spacing between grooves; w is the width of the groove valley; $\bar{p}$ is the actual surface pressure; p^* is the pressure needed for finger under the full contact condition (refer to Eqs. (4) and (5)). The Westergaard model also can be applied for the sliding contact of a rigid wavy surface with a viscoelastic half-space (Menga et al., 2014). A modified model is used in this paper to predict the actual surface pressure and the pressure needed for the fingertip under the full contact condition.

$$\bar{p} = \frac{F_N}{\pi a^2} \tag{4}$$

$$p^* = \pi E^* \frac{D}{2\lambda} \tag{5}$$

$$\frac{1}{E^*} = \frac{1 - v_{finger}^2}{E_{finger}} + \frac{1 - v_{surface}^2}{E_{surface}} \tag{6}$$

$$a = \sqrt[3]{\frac{3RF_N}{E^*}} \tag{7}$$

Where F_N is the applied load; a is the contact radius of the fingertip in contact with counter-surface predicted by Hertz equation; D is the depth of groove(amplitude); E^* is the effective Young's modulus; v_{finger} and $v_{surface}$ are the Poisson ratio of finger and counter-surface accordingly; R is the radius of fingertip.

The apparent contact area (A_{app}) is influenced by the contact condition which is determined by the pressure ratio $\left(\frac{\bar{p}}{p^*}\right)$. When the pressure ratio $\left(\frac{\bar{p}}{p^*}\right)$ is smaller than 1, the contact area of grooved channels is under the partial contact condition. When the pressure ratio $\left(\frac{\bar{p}}{p^*}\right)$ is larger than or equal to 1, the contact area of grooved channels is under the full contact condition.

The apparent contact area of grooved channels under the minimum partial contact ($A_{app,PC}$) and the full contact ($A_{app,FC}$) conditions are predicted as:

$$A_{app,PC} = \pi a^2 - Nw\bar{l} = N(\lambda - w)\bar{l}, \qquad \text{for } \bar{p} < p^* \tag{8}$$

$$A_{app,FC} = N(\lambda - w)\bar{l} + N\left[2\left(\sqrt{\left(\frac{w}{2}\right)^2 + D^2}\right)\right]\bar{l}, \qquad \text{for } \bar{p} \geqslant p^* \tag{9}$$

Where a is the contact radius of fingertip in contact with counter-surface predicted by Hertz equation (Eq. (7)); N is the number of grooves in contact; λ is the lambda spacing between grooves; w is the width of the groove valley; $\sqrt{\left(\frac{w}{2}\right)^2 + D^2}$ is an approximation to the slope of groove sides; $\bar{l}$ is the average length of the grooves in contact (refer to Fig. 5 a). As illustrated in Fig 5, under the same load, the contact condition between the fingertip and counter body depends on the depth of grooved textures. With deeper depth, the valley of the texture is not contacted. There is less contact area of skin under the partial contact condition compared to the full contact condition with shallow depth.

Parameters from literature (refer to Table 3) are used in the analytical model to estimate pressure ratio and contact area ratio (refer to Fig. 6). To better understand the contact condition such as partial or full contact, the fingertip is assumed to be flat. There is an upper limit for the contact ratio which can be predicted by the maximum contact area under the full contact (refer to Eq. (9)) over the contact area estimated by Hertz theory.

Table 3
Parameters from literature are used in the analytical model to estimate the contact ratio between finger and grooved channel (Maeno et al., 1998; Dandekar et al., 2003; Shao et al., 2010; Greaves et al., 2011).

	Values
E_{finger}	0.2 MPa
$E_{surface}$	150 GPa
υ_{finger}	0.48
$\upsilon_{surface}$	0.3
Depth of groove	30 μm, 15 μm, 5 μm

Fig. 6 (a) (c) and (e) show the relation between the pressure ratio $(\frac{\bar{p}}{p^*})$ and applied normal load (F_N) for the different depth of grooves (D). Fig. 6 (b) (d) and (f) show that estimated contact ratio is in direct proportion to the measured COF. When finger is under the partial contact condition $\left(\frac{\bar{p}}{p^*} < 1\right)$, the contact ratio is smaller than 1 (range from 0.30 to 0.41 for D = 30 μm; 0.50 to 0.72 for D = 15 μm). When finger is under the full contact condition $\left(\frac{\bar{p}}{p^*} \geqslant 1\right)$, the contact ratio can be greater than 1 (range from 1.06 to 1.44 for D = 5 μm) which is possible due to the combination area of the surface, groove sides and groove valley (bottom) of the counter-body when the pressure needed for finger under the full contact condition (p^*) is reached.

Skin friction arises from the interaction with the contact surface, and is directly related to the contact area. The grooved channels are able to reduce the apparent contact area (under the partial contact condition) or increase the apparent contact area (under the full contact condition) in order to affect the real contact area. For the partial contact $\left(\frac{\bar{p}}{p^*} < 1\right)$, the apparent contact area is mainly

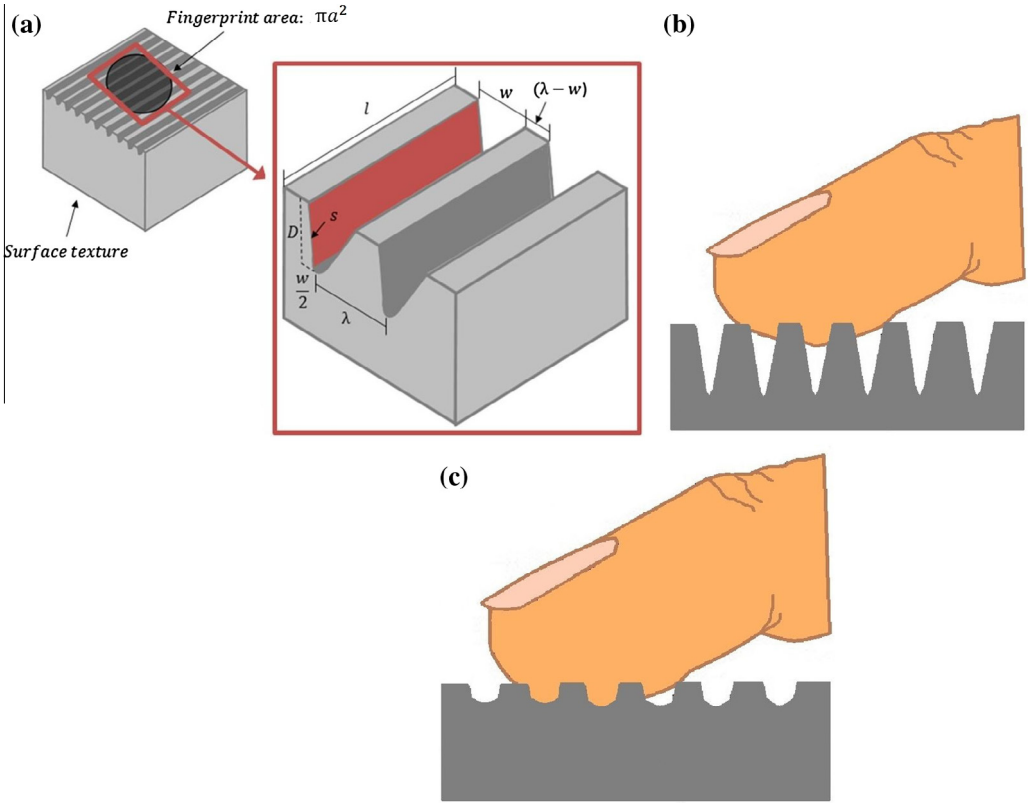

Fig. 5. (a) Parameters of grooved channel in contact; (b) partial contact and (c) full contact depends on the top to valley distance of the grooved channel.

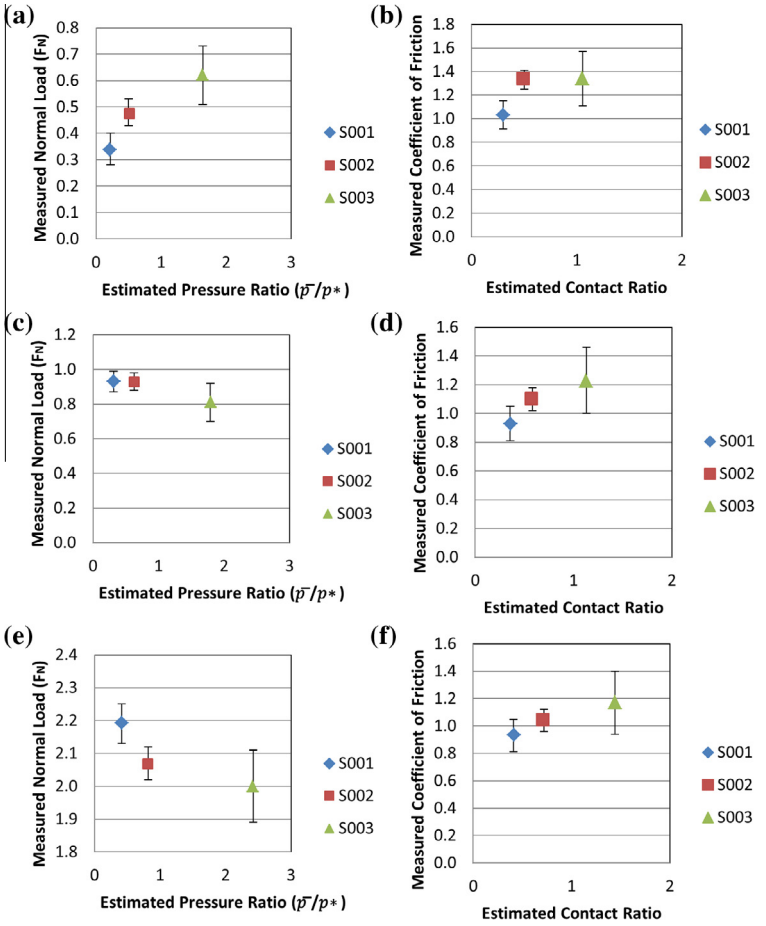

Fig. 6. Measured normal load vs. estimated pressure ratio at (a) F_N = 0.5 N, (c) F_N = 1 N, (e) F_N = 2 N; and measured COF vs. estimated contact ratio at (b) F_N = 0.5 N, (d) F_N = 1 N, (f) F_N = 2 N.

focused on the surface of the counter body (refer to Fig 5 b), and the reduction of the apparent contact area is up to approximately 60% by calculating the amount of area removed by grooved channels over the non-grooved surface apparent area (refer to Eq. (9)). On the contrary, when the pressure needed for finger under the full contact condition (p^*) is reached $\left(\frac{\bar{p}}{p^*} \geqslant 1\right)$, skin touches the combination area of the surface, groove sides and groove valley (bottom) of the counter body under the full contact condition (refer to Fig 5 c). The contact pressure is one key factor which directly affects the contact condition as the partial or full contact. The effect of contact condition is able to influence the friction force due to the change of apparent contact area. The real contact area is a fraction of apparent contact area, therefore, if apparent contact area is increasing, the real contact area increases accordingly (Zahouani et al., 2011). The adhesion component of the friction force increases when the real contact area increases (refer to Eq. (2)).

5.2. The effect of the sliding direction

From the experimental results described here, the relationship between COF of skin and load depends on the sliding direction as well. Perpendicular sliding has lower values in COF than parallel sliding for grooved channel (as shown in Fig. 4). This phenomenon has to do with viscoelastic behavior of skin, which causes deformation delay against the surface texture (Derler et al., 2007). As a result of deformation delay, the contacted skin region is under the partial contact condition due to the loop of deforming and bouncing against the grooved texture in perpendicular sliding (refer to Fig 7 a).

In addition, the hysteresis friction is added to the total friction as deformative component of friction force (Tomlinson et al., 2011). Greenwood and Tabor (Greenwood and Tabor, 1958) proposed a hysteresis friction model of a rigid conical slider moving along a soft elastomer like rubber. From the method, the hysteresis friction for a finger sliding along a ridged surface can be derived as:

$$\mu_h = \frac{\beta}{\pi} cot\theta \tag{10}$$

Where μ_h is the coefficient of friction due to hysteresis; β is the viscoelastic loss fraction due to hysteresis; θ is the hysteresis of contact angles (the angle which the conical indenter makes with the vertical centre line). In our case, the high portions of the samples on top of the grooves act as the ridges. This hysteresis friction model can be applied to grooved textures in perpendicular sliding.

The skin deformed against the edges along the length *dl*, and the force (W) due to the pressure of the ridge is predicted as (Tomlinson et al., 2011):

$$W = \int p\, L\, dl \tag{11}$$

Where p is the pressure along the contact area of the ridge and skin; L is the length of the ridge in contact. $dt = dl\ sin\ \theta$ is the distance from central axis (t) between the limits of 0 and a, and hysteresis force (F_{hys}) is the horizontal component of the applied

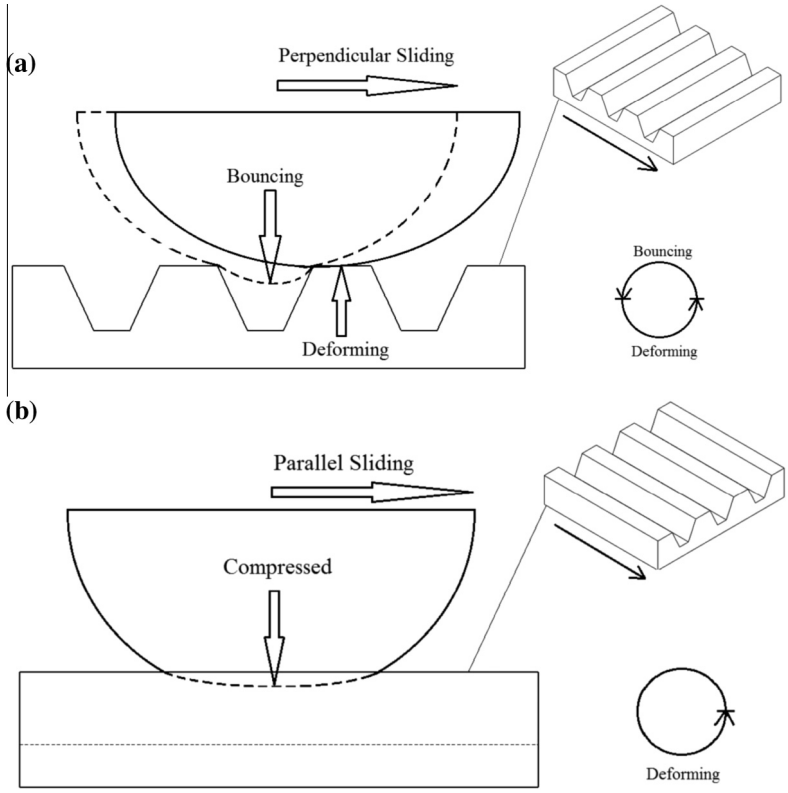

Fig. 7. Schematic diagram of (a) perpendicular sliding and (b) parallel sliding.

pressure (W). Based on this approach, which was slightly adapted to the current case, the pressure and the resulting hysteresis force (F_{hys}) along the leading edge can be determined as follows:

$$F_{hys} = W.cos\theta = \int_0^s \int_0^a p.L.cot\theta.dt.ds = \frac{F_N}{2}cot\theta \tag{12}$$

Where dt is the distance from the central axis (t); ds is the distance of the apparent contact width (refer to Fig 8).

The normal force (F_N) applied on the single 3D trapezoidal ridge is described as follows:

$$F_N = \int_0^s 2 \int_0^a p.L.dt.cot\theta.ds \tag{13}$$

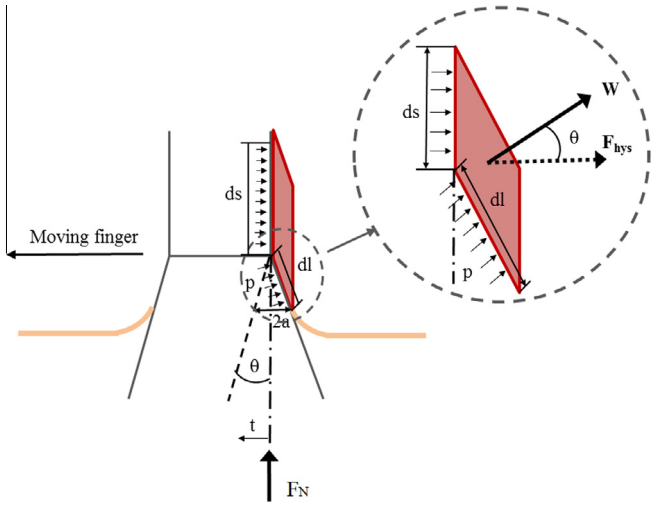

Fig. 8. Schematic of ridge-skin contact model.

Combined with experimental data and prediction of analytical model (based on Eq. (13)) Tomlinson concludes that once the applied loads are greater (normal load > 1 N) with larger ridges (ridge height > 105 μm), interlocking and hysteresis frictions have a large percentage of the overall friction (Tomlinson et al., 2011). But for small ridges (ridge height < 33.5 μm), interlocking and hysteresis frictions have little influence on the total friction and can almost be neglected when ridge height is as small as 4.75 μm.

In our case, the depths of grooves are 30 μm, 15 μm and 5 μm and hysteresis friction has limited influence of the overall friction. Also, the loop of deforming and bouncing against the grooved texture (perpendicular sliding) can only touch the leading edge of the ridge. The trailing edge of the ridge is not contact by the fingertip during the loop. Therefore, the full contact condition is not reached for perpendicular sliding. Under the partial contact condition, the contact area decreases and the adhesion component of friction force decreases accordingly (refer to Section 5.1). The adhesion component of friction has the largest influence on the total measured friction. This conclusion is consistent with other experimental studies which suggest that adhesion friction has the dominant role in skin friction (Wolfram, 1983; Asserin et al., 2000; Koudine et al., 2000; Sivamani et al., 2003; Adams et al., 2007; Tang et al., 2008; van Kuilenburg et al., 2012; Veijgen et al., 2013). Therefore, even with the contribution of hysteresis friction, the total friction decreases due to the decrease of adhesion force in perpendicular sliding.

On the contrary, when the pressure needed for the full contact condition (p^*) is reached during parallel sliding, the contacted skin region is under the full contact condition without undergoing the hysteresis loop of deforming and bouncing (refer to Fig 7 b). Therefore, parallel sliding generates more real contact area compared to perpendicular sliding for grooved channel, and as a result, higher friction force is observed in parallel sliding direction. In addition, the friction force is smaller for the deterministic structures in

perpendicular sliding compared to stochastic surface because of reduced contact area as well (refer to Fig. 3 b).

6. Conclusions

In this research, friction of fingertip was measured against deterministic surface structures, i.e. grooved channels on the steel samples. Based on the experimental results, the role of groove depth and sliding direction are investigated for the grooved channels. The greater depth of grooved channel is able to reduce the apparent contact area under the partial contact condition, however, the apparent contact area is increased under the full contact condition. And, the real contact area varies as a fraction of apparent contact area. As a result, the adhesion component of friction can be directly influenced under different contact condition.

The sliding direction is another key factor to consider when measuring friction. During parallel sliding, a higher friction force was observed due to the increased contact area for grooved channels. On the contrary, in perpendicular sliding lower friction was obtained including limited contribution of the deformation component due to hysteresis. The contacted skin region is under the partial contact condition due to the loop of deforming and bouncing against the grooved texture in perpendicular sliding. Furthermore, a comparison between deterministic and stochastic samples validated the effect of directionality on tactile friction.

This experimental research contributes to the haptic perception related research, and to the development of other direction-dependent surface structures for touch like: straight line, curve and chevron texture (v-shaped pattern).

Acknowledgements

This work was supported by the Research Programme of the Research Fund for Coal and Steel, contract no. RFSR-CT-2011-00022. Special thanks to Gert-willem Romer for the equipment of laser surface texturing used for sample production, and gratefully acknowledge Dr. Marc Masen for patient and scholarly discussions.

References

Adams, M.J., Briscoe, B.J., Johnson, S.A., 2007. Friction and lubrication of human skin. Tribol. Lett. 26 (3), 239–253.
Asserin, J., Zahouani, H., Humbert, Ph., Counturaud, V., Mougin, D., 2000. Measurements of the friction coefficient of the human skin in vivo: quantification of the cutaneous smoothness. Colloids Surf. B: Biointerfaces 19, 1–12.
Barnes, C.J., Childs, T.H.C., Henson, B., Southee, C.H., 2004. Surface finish and touch – a case study in a new human factors tribology. Wear 257, 740–750.
Bowden, F.P., Tabor, D., 1950. The Friction and Lubrication of Solids. Cambridge University Press, Oxford.
Cua, A.B., Wilhelm, K.P., Maibach, H.I., 1990. Frictional properties of human skin: relation to age, sex and anatomical region, stratum corneum hydration and trans epidermal water loss. Br. J. Dermatol. 123, 473–479.
Dandekar, K., Raju, B.I., Srinivasan, M.A., 2003. 3-D finite-element models of human and monkey fingertips to investigate the mechanics of tactile sense. J. Biomech. Eng.-Trans. ASME 125 (5), 682–691.
Darden, M.A., Schwartz, C.J., 2013. Investigation of friction mechanisms during the sliding of elastomers against hard parallel-ridge textures. Tribol. Int. 63, 2–7.
Derler, S., Huber, R., Feuz, H.P., Hadad, M., 2009. Influence of surface microstructure on the sliding friction of plantar skin against hard substrates. Wear 267, 1281–1288.
Derler, S., Gerhardt, L.-C., 2012. Tribology of skin: review and analysis of experimental results for the friction coefficient of human skin. Tribol. Lett. 45, 1–27.
Derler, S., Rotaru, G.-M., Ke, W., El Issawi-Frischknecht, L., Kellenberger, P., Scheel-Sailer, A., Rossi, R.M., 2014. Microscopic contact area and friction between medical textiles and skin. J. Mech. Behav. Biomed. Mater. 38, 114–125.
Derler, S., Schrade, U., Gerhardt, L.-C., 2007. Tribology of human skin and mechanical skin equivalents in contact with textiles. Wear 263, 1112–1116.
Diridollou, S., Vabre, V., Berson, M., Vaillant, L., Black, D., Lagarde, J.M., Grégoire, J.M., Gall, Y., Patat, F., 2001. Skin ageing: changes of physical properties of human skin in vivo. Int. J. Cosmet. Sci. 23, 353–362.
Edwards, C., Marks, R., 1995. Evaluation of biomechanical properties of human skin. Clinics Dermatol. 13, 375–380.
Fagiani, R., Massi, F., Chatelet, E., Costes, J.P., Berthier, Y., 2012. Contact of a finger on rigid surface and textiles: friction coefficient and induced vibrations. Tribol. Lett. 48, 145–158.
Gee, M.G., Tomlins, P., Calver, A., Darling, R.H., Rides, M., 2005. A new friction measurement system for the frictional component of touch. Wear 259, 1437–1442.
Greenwood, J.A., Tabor, D., 1958. The friction of hard sliders on lubricated rubber: the importance of deformation losses. Proc. Phys. Soc. 71 (6), 989–1001.
Heinrich, U., Koop, U., Lenveu-Duchemin, M.-C., Osterrieder, K., Bielfeldt, S., Chkarnat, C., Degwert, J., Hantschel, D., Jaspers, S., Nissen, H.-P., Rohr, M., Schneider, G., Tronnier, H., 2003. Multicentre comparison of skin hydration in terms of physical-, physiological- and product-dependent parameters by the capacitive method (Corneometer CM 825). Int. J. Cosmet. Sci. 25, 45–53.
Hendriks, C.P., Franklin, S.E., 2010. Influence of surface roughness, material and climate conditions on the friction of human skin. Tribol. Letters 37, 361–373.
Liu, X., Yue, Z., Cai, Z., Chetwynd, D.G., Smith, S.T., 2008. Quantifying touch – feel perception: tribological aspects. Meas. Sci. Technol. 19, 1–9.
Johnson, K.L., Greenwood, J.A., Higginson, J.G., 1985. The contact of elastic regular wavy surface. Int. J. Mech. Sci. 6, 383–396.
Johnson, S.A., Gorman, D.M., Adams, M.J., Briscoe, B.J., 1993 (The friction and lubrication of human stratum corneum). Proceedings 19th Leeds-Lyon Symposium on Tribology. Elsevier, ISBN 9780444897893, pp. 663–672.
Klatzky, R.L., Pawluk, D., 2013. Haptic perception of material properties and implications for applications. Proc. IEEE 101, 2081–2092.
Koudine, A., Barquins, M., Anthoine, P.H., Aubert, L., Leveque, J.L., 2000. Friction properties of skin: proposal of a new approach. Int. J. Cosmet. Sci. 22, 11–20.
Kuramitsu, K., Nomura, T., Nomura, S., Maeno, T., Nonomura, Y., 2013. Friction evaluation system with a human finger model. Chem. Lett. 42, 284–285.
Lapière, C.M., 1990. The ageing dermis: the main cause for the appearance of 'old' skin. Br. J. Dermatol. 122, 5–11.
Liu, X., Yue, Z., Cai, Z., Chetwynd, D.G., Smith, S.T., 2008. Quantifying touch-feel perception: tribological aspects. Meas. Sci. Technol. 19, 084007.
Maeno, T., Kobayashi, K., Yamazaki, N., 1998. Relationship between the structure of human finger tissue and the location of tactile receptors. JSME Int. J. Ser. C-Mech. Syst. Mach. Elem. Manuf. 41 (1), 94–100.
Menga, N., Putignano, C., Carbone, G., Demelio, G.P., 2014. The sliding contact of a rigid wavy surface with a viscoelastic half-space. Proc. R. Soc. A: Math. Phys. Eng. Sci. 470, 1–14.
Morales Hurtado, M., Zeng, X., van der Heide, E., 2014 (The Human skin and hydration). In: Yoshitaka, Nakanishi (Ed.), Hydrated Materials: Applications in Biomedicine and the Environment. Pan Stanford Publishing Pte. Ltd, ISBN 978-981-4316-31-6, Copyright © 2015.
Ramsay, T.G., 1996. Fat cells. Endocrinol. Metab. Clinics North Am. 25, 847–870.
Shao, F., Childs, T.H.C., Barnes, C.J., Henson, B., 2010. Finite element simulations of static and sliding contact between a human fingertip and textured surfaces. Tribol. Int. 43, 2308–2316.
Silver, F.H., Kato, Y.P., Ohno, M., Wasserman, A.J., 1992. Analysis of mammalian connective tissue: relationship between hierarchical structures and mechanical properties. J. Long-term Eff. Med. Implants 2, 165–198.
Sivamani, P.K., Goodman, J., Gitis, N., Maibach, H.I., 2003. Friction coefficient of skin in real-time. Skin Res. Technol. 9, 235–239.
Skedung, L., Danerlov, K., Olofsson, U., Johannesson, C.M., Aikala, M., Kettle, J., Arvidsson, M., Berglund, B., Rutland, M.W., 2011. Tactile perception: finger friction, surface roughness and perceived coarseness. Tribol. Int. 44, 505–512.
Smith, A., Chapman, C., Deslandes, M., Langlais, J., Thibodeau, M.-P., 2002. Role of friction and tangential force variation in the subjective scaling of tactile roughness. Exp. Brain Res. 144, 211–223.
Steinhoff, K., Rasp, W., Pawelski, O., 1996. Development of deterministic-stochastic surface structures to improve the tribological conditions of sheet forming processes. J. Mat. Process. Technol. 60, 355–361.
Tagami, H., Yoshikuni, K., 1985. Interrelationship between water-barrier and reservoir functions of pathologic stratum corneum. Arch. Dermatol. 121, 642–645.
Tang, W., Ge, S., Zhu, H., Cao, X., Li, N., 2008. The influence of normal load and sliding speed on frictional properties of skin. J. Bionic Eng. 5, 33–38.
Taylor, M., Lederman, S., 1975. Tactile roughness of grooved surfaces: a model and the effect of friction. Percept. Psychophys. 17 (1), 23–36.
Tomlinson, S.E., Lewis, R., Carré, M.J., 2009. The effect of normal force and roughness on friction in human finger contact. Wear 267, 1311–1318.
Tomlinson, S.E., Carre, M.J., Lewis, R., Franklin, S.E., 2011. Human finger contact with small, triangular ridged surfaces. Wear 271, 2346–2353.
van Kuilenburg, J., Masen, M.A., Groenendijk, M.N.W., Bana, V., van der Heide, E., 2012a. An experimental study on the relation between surface texture and tactile friction. Tribol. Int. 48, 15–21.
van Kuilenburg, J., Masen, M.A., van der Heide, E., 2012b. Contact modeling of human skin: what value to use for the modulus of elasticity. J. Eng. Tribol. 227 (4), 349–361.
van Kuilenburg, J., Masen, M.A., van der Heide, E., 2013. A review of fingerpad contact mechanics and friction and how this affects tactile perception. Proc. Inst. Mech. Eng. J J. Eng. Tribol., 1–16.
van der Heide, E., Zeng, X., Masen, M.A., 2013. Skin tribology: science friction? Friction 1 (2), 130–142.
Veijgen, N.K., Masen, M.A., van der Heide, E., 2013a. Variables influencing the frictional behaviour of in vivo human skin. J. Mech. Behav. Biomed. Mater. 28, 448–461.

Veijgen, N.K., Masen, M.A., van der Heide, E., 2013b. Relating friction on the human skin to the hydration and temperature of the skin. Tribol. Lett. 49, 251–261.
Wang, Q., Hayward, V., 2008. Tactile synthesis and perceptual inverse problems seen from the viewpoint of contact mechanics". ACM Trans. Appl. Percept. 5 (2), 2–19.
Westergaard, H.M., 1939 (Bearing pressures and cracks). J. Appl. Mech. Trans. ASME, 49–53.
Wolfram, L., 1983. Friction of skin. J. Soc. Cosmet. Chem. 34, 465–476.
Zahouani, H., Ben Tkaya, M., Mezghani, S., Pailler-Mattei, C., 2011. Adhesive contact in the context of multi-asperity interaction. C. R. Mec. 339, 502–517.